Composition-Controlled Structure and Colloidal Stability of Surfactant-Free Gold-Copper Alloy Nanoparticles Synthesized by Picosecond Laser Ablation in Liquid

Jasim Al-Zanganawee[1], Hind Waleed Abdullah[1], Sarah Abbas Jasim[1], Tahseen Hussein Mubarak[1], Sorina Iftimie[2] and Oana Brincoveanu[3]
[1]*Department of Physics, University of Diyala, Al-Shaheed Ark Mosque Str. 22, 32001 Baqubah, Iraq*
[2]*Faculty of Physics, University of Bucharest, Atomistilor Str. 405, 077125 Măgurele, Romania*
[3]*National Institute for Research and Development in Microtechnologies, 077125 Bucharest, Romania*
Alzanganawee@uodiyala.edu.iq, Hindwaleed@uodiyala.edu.iq, sarahabbas@uodiyala.edu.iq, prof.dr.tahseen@uodiyala.edu.iq, sorina.iftimie@unibuc.ro, oana.brincoveanu@imt.ro

Keywords: PPLAL, Au-Cu Alloy Nps, Colloidal Stability, Vegard's Law.

Abstract: By using picosecond laser ablation in water. (PPLAL) (λ-1064 nm, E=500 mJ, and Pulse=2000), we made colloidal nanoparticles of gold (Au) and Au-Cu alloys in DI water. The impact of (Au) and Au-Cu alloys compositions on structure, particle morphology, and nanocolloidal stability was thoroughly examined. X-ray diffraction verified a single-phase fcc solid-solution across all compositions, with the (111) peak changing consistently from 38.77° (Au) to 41.55° ($Au_{50}Cu_{50}$), corresponding with Vegard-like lattice contraction from ~0.402-0.406 nm (Au) to ~0.376-0.380 nm (Cu-rich alloys). Scherrer analysis demonstrated that the crystallite sizes got more smaller depending on the alloy composition, varying from about 26 nm for (pure Au) to about 11-17 nm for Cu- excess alloys. FESEM imaging and size histograms showed that the particles spread out in a U-shape: pure Au made spherical nanoparticles that were very close together (median ≈ 47 nm), low Cu content (12.5-25 at.%) made the particles stick together and spread out more (≈ 72-81 nm), and higher Cu fractions (40-50 at.%) made the particles smaller and more uniform. Electrophoretic light scattering revealed that the surface charge could be changed by changing the composition. It went from very negative (−42.5 mV, Au) to almost neutral (+5-10 mV, mid-range Cu), and then back to substantially negative at $Au_{50}Cu_{50}$ (−23.9 mV). Dynamic light scattering showed even more clearly that there was a lot of aggregation at intermediate Cu concentrations. UV-Vis spectra show an Au LSPR at 521 nm, while alloy samples exhibit red-shifted plasmon peaks at 568 nm (AuCu12.5), 579 nm (AuCu25), 614 nm (AuCu40), and 607 nm (AuCu50.These findings indicate that alloy composition is an effective means of regulating lattice contraction, nanocrystallinity, and colloidal stability in surfactant-free Au-Cu colloids generated by PPLAL.

1 INTRODUCTION

Bimetallic nanoparticles (BNPs) are essentially two different metals that exhibit unique interaction properties, which can significantly enhance the properties of the particles. Therefore, this type of nanoparticle has received wide attention from researchers specializing in scientific and technological fields, as the concept of nanoparticles refers to solid-state particles with a size of less than 100 nanometers [1]. Such bimetallic nanoparticles as Au-Ag [2], AuCu [3], AuPd, PtPd, and PtCu [4], and so on. Au-Cu alloy nanoparticles have recently emerged as a potential alloy nanoparticle system, demonstrating exceptional applications such as in catalysis, light harvesting [5], sensing [6], and photothermal antibacterial and Wound Healing (WH) [7]. Gold-Copper Bimetallic nanoparticles exhibit greater structural tunability and functional versatility compared to their monometallic counterparts (Au or Cu) [8]. There are many method have been used for synthesis Au-Cu BNPs such as chemical method including co-reduction [9], Seed-Mediated [5], Galvanic Replacement [10], On the other hand, these techniques frequently include the utilization of surfactants, organic stabilizers, or hazardous chemicals, all of which have the potential to leave behind undesired residues, introduce

contaminants, or restrict surface accessibility. Physical approaches, such as laser ablation, provide superior control (particle size, shape), homogeneity and reactivity, particularly for applications that require ligand-free surfaces to be present [11]. Pulsed laser ablation in liquid has become one of the approved physical methods for synthesizing colloidal nanoparticles with different compositions such as metals, alloys, oxides, and hydroxides, etc. This method depends on the interaction of the laser in the form of very short pulses with the metal target placed inside the liquid [12]-[14]. In addition, the pulsed laser ablation method in liquid can create nanostructures of different shapes, such as nanoparticles (e.g., gold and silver nanoparticles [15]), nanotubes (e.g., carbon nanotubes [16]), nanorods [13], and nanocomposites [17]. The properties of nanoparticles prepared by PLAL are greatly affected by the duration of the laser pulse incident on the target. Therefore, the pulse duration affects the process of the laser energy incident on the target and the subsequent dynamics of plasma expansion. picosecond ablation is particularly attractive, since it minimizes heat diffusion into the target and favors rapid nucleation, leading to smaller crystallites and better structural uniformity compared with nanosecond or femtosecond regimes [13], [18]. Even with these benefits, there aren't many systematic investigations on how the composition of Au-Cu nanoparticles made by picosecond LAL changes over time. Initial investigations have shown that it is possible to make Au-Cu alloys using laser ablation [19], but this research has mostly concentrated on showing that synthesis was possible rather than linking alloy composition to crystal structure, morphology, and colloidal stability. This work concerns on the fabrication of nanocolloids of pure Au and Au-Cu nanoalloys with different Cu concentration ratios using the (PPLAL) approach. A Nd:YAG laser working conditions at λ = 1064 nm, with a 500 mJ per pulse and 550-ps laser pulse, was used to synthesis the nano-colloids directly from bulk pure Au and Au-Cu metallic targets. Careful attention is given to how the Cu ratios impact on the "crystal structural, morphological, and nano-colloidal" features of the synthesizing nanoparticles. The checking involves analysis of alloy composition and crystallite size by XRD and EDX, and particle morphology and size by SEM, as well as surface charge and hydrodynamic behavior measurements. Although numerous studies have been conducted on the preparation of gold and copper nanoparticles using pulsed laser ablation in water, most of these studies focus on the feasibility of manufacturing these particles. The reliance on single-particle structures for these nanoparticles is limited and insufficient, and the colloidal shape and stability of nanoparticles produced by ultrafast (picosecond) laser ablation are not well understood. This aspect remains understudied, making it crucial to address this gap. Synthesizing bond-free bimetallic nanoparticles can be utilized in various applications, including catalysis, antibacterial properties, decolorization, and others.

2 MATERIALS AND METHODS

2.1 Experimental

In the experimental part, metallic targets of gold and gold-copper alloys with different copper-to-gold ratios of 0%, 12.5%, 25%, 40%, and 50% were prepared by smelting high-purity 99.999% gold and copper together at temperatures over 1000°C. They were cast in a disc form with a radius of 0.5 cm and a height of less than 0.1 cm. The surfaces of the metallic targets were polished with zero-gauge sandpaper, then washed with dishwashing liquid, rinsed with normal water, and then washed with DI water. The targets were then placed in a glass container filled with distilled water inside an ultrasonicator for five minutes. All impurities were removed from the metal targets by repeating the sonication process step two times, first with ethyl alcohol (CH3CH2OH) and again with dimethyl ketone ($(CH_3)_2CO$). In order avoid any contamination, the Pure Au and AuCu alloys targets were saved in clean containers. In this work, a picosecond laser system (Model A0508, Picosure type) was used as a picosecond laser source for ablation. The wavelengths that can be selected are 1064, 532, 755, and 1320 nm, and the pulse duration is in the picosecond region, which is around 550 ps. Specifically, the laser was set up to produce 2000 pulses at a repetition frequency of 1 Hz, with an E= 500 mJ per pulse, a wavelength of 1064 nm, and a spot width of approximately 1 mm for the current study. Colloidal nanoparticles of pure gold and gold-copper alloys (12.5%, 25%, 40%, and 50% copper by composition) were synthesized by laser ablation of the corresponding metal targets. A 5 mL glass beaker containing 5 mL of DI water was used for each target, with the water level (height) kept 51 mm above the surface of the Au and AuCu alloys target. A picosecond pulsed laser with a 1064 nm wavelength, 500 mJ pulse energy, and 1 Hz

repetition frequency was used for ablation. The pulse duration was 550 ps, and the laser beam was focused at a distance of 9.5 cm from the target, producing a spot size of approximately 1 mm on the surface. To prevent local overheating and melting, the beaker was rotated continuously during the ablation process. Each sample was irradiated with a total of 2000 pulses over 93 minutes, delivered in cycles of 100 pulses within 100 seconds, followed by a 3-minute pause to minimize water evaporation, prevent excessive heating, and reduce nanoparticle agglomeration. Following irradiation, colloidal suspensions of gold and gold-copper nanoparticles were obtained in the liquid medium, as illustrated in Figure 1. The names of the colloidal Au and AuCu alloy nanoparticles were Au, AuCu12.5, AuCu25, AuCu40, and AuCu50.

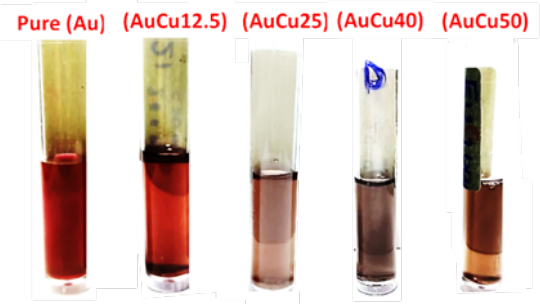

Figure 1: Colloidal suspensions of pure au and au-cu alloy nanoparticles synthesized by picosecond pulsed laser ablation in liquid (PPLAL).

3 RESULTS AND DISCUSSION

3.1 XRD Analysis

The XRD patterns in Figure 2 demonstrate that all colloidal nanoparticles made by PPLAL at 1064 nm, 500 mJ, and 2000 pulses crystallize in the fcc (Fm-3m) structure, which has the (111), (200), (220), and (311) reflections. As the Cu content increases, the (111) peak moves from 38.77° for pure Au to 41.55° for AuCu50. This shows that the interplanar spacing (d111) is getting smaller and the lattice is getting smaller in a way that is compatible with substitutional Au-Cu alloying and Vegard-like behavior [20]-[22]. As shown in Table 1, the lattice parameter goes down from about 0.402-0.406 nm (Au) to about 0.376-0.380 nm for Cu-richer alloys. At the same time, the peak broadening goes up and the Scherrer crystallite sizes go down from about 25.7 nm (Au) to about 11-17 nm across the alloy series (for example, about 17.4 nm for AuCu12.5 and about 10.8-15 nm for Au75-Au50) [20]-[22]. The lack of supplementary reflections associated with Cu, oxides, or ordered superlattice phases corroborates the existence of single-phase, nanocrystalline Au-Cu solid solutions within the examined compositions [21], [23]. Crystal volumes were calculated by Scherer's equation.[24].

$$D = k\lambda/(\beta \cos \theta \quad) \tag{1}$$

Where "D is the crystal size, λ(1.54 Å) is the wavelength of the incident beam, k is the shape factor, β is the full width half-maximum (FWHM) and θ is the Bragg diffraction angle".We used the following formula to find the FCC lattice constant of pure Au and AuCu BNPs [25]:

$$a = d/(h2 + K2 + l2)1/2. \tag{2}$$

Where: "a' is the lattice constant (hkl) and Miller indices", and the calculated data are shown in Table 1. Bragg's law uses the following formula to figure out the path difference between two beams and its multiple of the wavelength [26]:

$$n\lambda = 2d\_(hkl\ ) \ Sin\theta. \tag{3}$$

3.2 FESEM Results

FE-SEM images in Figure 3, show that all Au-Cu nanoparticles synthesized by picosecond laser ablation in water (PPLAL, 550 ps) are generally near-spherical and well-dispersed, although the degree of aggregation and the uniformity of shape vary with Cu content. For the pure Au sample (Fig. 3a), particles are predominantly isolated, spherical, and exhibit a narrow size distribution. Adding a Cu material with low contents from 12.5% to 25 %as showning in Figure 4b, c lead to increase in mean particle diameter and a broader range of sizes, as showning in Figure 3a, b, which usually occurring by further agglomerated or molted materials, steady with improve coalescence through PPLAL in liquid (water) [19], [27], [13]. When the prencentage ratio of Copper (Cu) inside Au alloy from the 40 % to 50% (Fig. 3d, e), the diameter (size of particle) will decreases regarding the pure-Au value. Figure 4 shows the particle diameter D and area distributions of Pure Au Colloidal and four different compositions of AuCu colloidals.The change in morphology suggests a composition-dependent nucleation and growth mechanism under picosecond ablation conditions, where mid-range Cu promotes particle-particle coalescence, while higher Cu stabilizes smaller alloyed nuclei with more regular shapes [19], [27]. These morphological observations are in agreement with the XRD results

(Fig. 2), which show (111) peak shifts to higher 2θ and decreasing lattice parameters, indicative of solid-solution Au-Cu alloy formation [27]. Furthermore, EDS elemental mapping (Fig. 4) confirms the co-localization of Au and Cu within individual nanoparticles, ruling out large-scale phase segregation [19], [27].

3.3 Histogram Analysis

The particle-size histograms (Fig. 4) and the summary statistics (Table 2) illustrate a distinct, composition-dependent evolution in size distribution for Au to Au-Cu alloy nanoparticles. Pure Au shows the narrowest distribution (median ≈ 47 nm, σ ≈ 7.4 nm), which aligns with FESEM images (Figure 3a) showing uniform, well-dispersed spherical particles. Adding a small Cu fraction widens both the mean and distribution (median ≈ 80-81 nm, σ ≈ 16-19 nm), reflecting FESEM observations of partial agglomeration (Fig. 3b, c). As Cu content increases further (AuCu40 and AuCu50), the median and spread reduce again-matching the more regular, less aggregated morphology in FESEM (Fig. 3d, e). This "U-shaped" behavior in dispersion is likely tied to colloidal stability modulated by composition and alloying [28]. In laser-ablated alloy systems, similar composition-dependent broadening of histograms has been linked to competitive nucleation and growth dynamics [29], while controlled particle size via adjusting composition has also been noted in LAL-synthesized alloy colloids [30]. Furthermore, FESEM-based elemental mapping in similar laser-ablated bimetallic nanoparticles highlights how alloy homogeneity and particle aggregation patterns reflect synthesis parameters and composition effects [31]. Thus, histogram metrics and imaging together affirm that Cu content governs not only average size but colloidal behavior and microstructure during and after ablation in liquid.

3.4 EDX Analysis

EDX spectra and elemental mapping confirm that pure Au contains only Au, while all Au-Cu samples display both Au and Cu homogeneously distributed within individual nanoparticles, consistent with uniform elemental co-localization in Au-Cu nanoalloys [27].

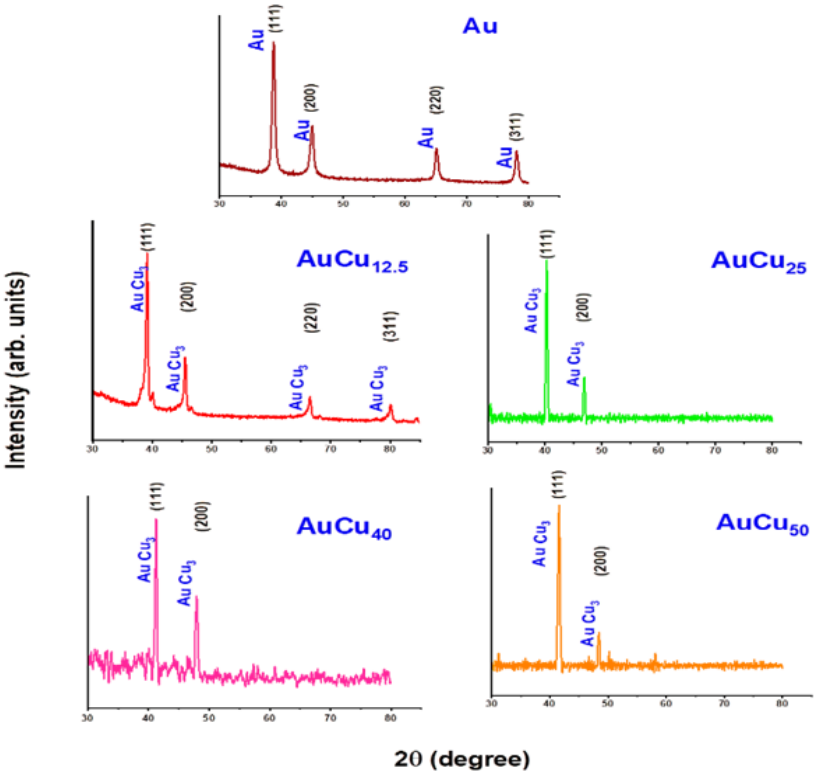

Figure 2: XRD plots of synthesis Au and AuCu colloidal nanoparticles by picosecond ablation in water (PPLAL).

Table 1: XRD parameters results of synthesis Au and AuCu colloidal nanoparticles by picosecondablation in water (PPLAL).

Sample Name	2 Theta (°)	hkl	d_{hkl} (Å)	FWHM (°)	Lattice constant a (Å)	Crystallite size D_{hkl} (nm)	Average crystallite size D (nm)
Au	38.768	111	2.3228	0.2489	4.0228	35.325	25.737
	44.956	200	2.0160	0.3589	4.0322	25.009	
	65.151	220	1.4320	0.5191	4.0496	18.960	
	78.115	311	1.2230	0.4516	4.0578	23.652	
AuCu12.5	39.05	111	2.3064	0.5195	3.9920	16.939	17.415
	45.39	200	1.9978	1.0391	3.9930	8.6519	
	66.44	220	1.4070	0.5195	3.9770	19.08	
	80.077	311	1.1981	0.5195	3.9710	20.85	
	84.39	113	1.1477	0.5195	3.8040	21.55	
AuCu25	40.323	111	2.2370	0.5196	3.8709	17.00449	15.028
	46.932	200	1.9360	0.6927	3.8688	13.05317	
AuCu40	41.069	111	2.1978	1.0391	3.80361	8.52358	10.810
	47.837	200	1.8999	0.6927	3.7998	13.0978	
AuCu50	41.552	111	2.1716	1.0391	3.7613	8.53714	10.832
	48.436	200	1.8778	0.6927	3.7550	13.1284	

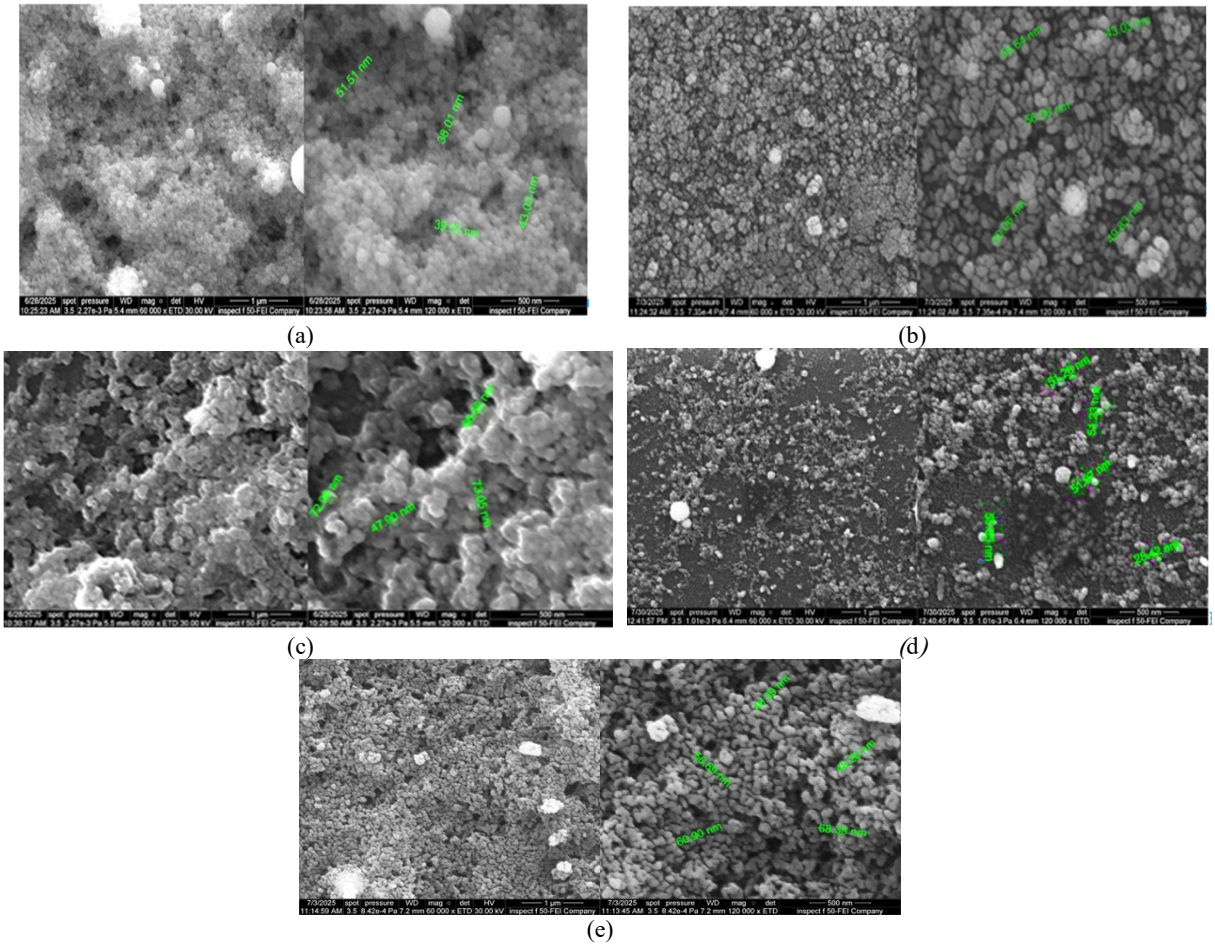

Figure 3: FESEM micrographs of Au and Au–Cu nanoparticles synthesized by PLAL and PPLAL at a laser wavelength of 1064 nm and a pulse energy of 500 mJ: a) Au nanoparticles synthesized by PLAL; b) AuCu12.5 nanoparticles synthesized by PPLAL; c) AuCu25 nanoparticles synthesized by PPLAL; d) AuCu40 nanoparticles synthesized by PPLAL; and e) AuCu50 nanoparticles synthesized by PPLAL.

This compositional homogeneity supports the XRD results, which show a single-phase fcc structure across all compositions. The systematic shift of the (111) peak from 38.77° (Au) to 41.55° (AuCu50) corresponds to a progressive decrease in lattice parameter from ~0.402-0.406 nm to ~0.376-0.380 nm, caused by substitutional incorporation of smaller Cu atoms into the Au lattice [27], [19]. This monotonic contraction follows the trend predicted by Vegard's law, which relates the lattice constant of an alloy to the weighted average of its constituents' lattice constants [29].

The concurrent reduction in Scherrer crystallite size from ~25.7 nm (Au) to ~11-17 nm for Cu-rich alloys, and the absence of secondary peaks, confirm the formation of homogeneous Au-Cu solid solutions without detectable phase segregation [30], [31].

3.5 Zeta Potential Measurement

Zeta potential Plots (Fig. 5) and electrophoretic mobility measurements (Table 3) reveal that pure Au nanoparticles have the highest magnitude surface charge (−42.47 mV; −3.32 μm•s^{-1}•(V/cm)$^{-1}$), which indicates excellent colloidal stability and strong electrostatic repulsion. The surface charge magnitude decreases with the addition of Cu: AuCu12.5 (−20.77 mV; −1.62 μm•s^{-1}•(V/cm)$^{-1}$) and AuCu25 (+5.00 mV; +0.39 μm•s^{-1}•(V/cm)$^{-1}$) approach instability, which is consistent with an increased tendency to aggregate. While AuCu50 (−23.85 mV; −1.86 μm•s^{-1}•(V/cm)$^{-1}$) partially recovers negative charge, higher Cu content (AuCu40, +10.13 mV; +0.79 μm•s^{-1}•(V/cm)$^{-1}$) maintains low electrostatic stabilization, indicating composition-dependent changes in surface chemistry.

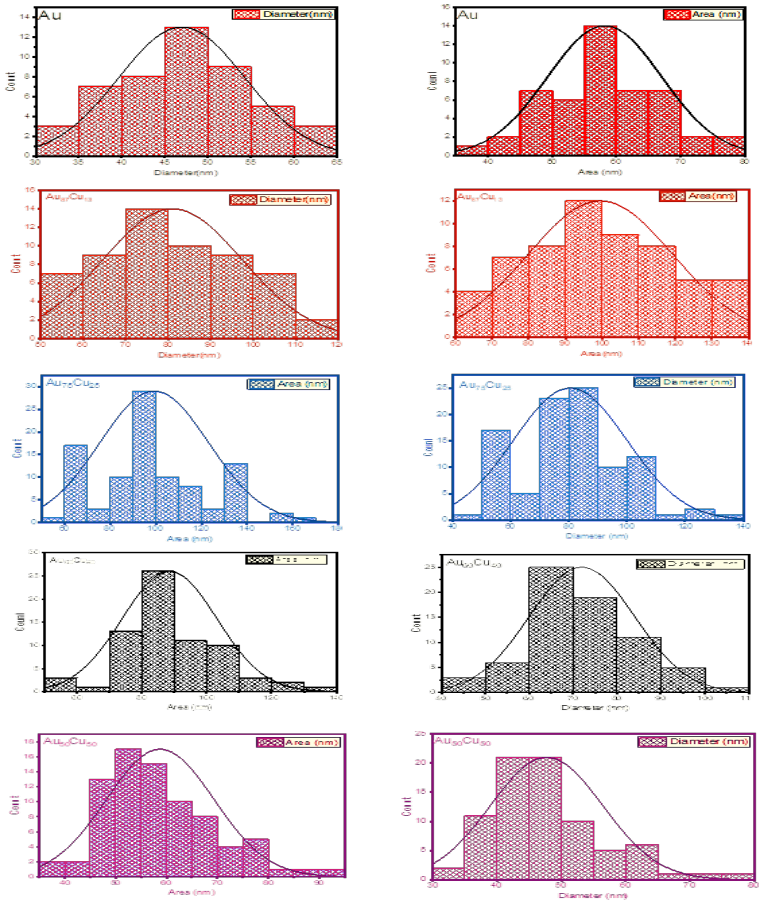

Figure 4: Particle size and projected area distributions of Au and Au–Cu nanoparticles synthesized by picosecond pulsed laser ablation in liquid (PPLAL)

Table 2: Statistical parameters of particle size and projected area distributions for Au and Au–Cu nanoparticles synthesized by PPLAL.

Sample	Metric	N total	Mean	Std. Dev.	Sum	Min	Median	Max
Au	Area (nm²)	103	71.15751	9.755	7329.224	50.887	75.604	94.505
Au	Diameter (nm)	48	46.97	7.355	2254.74	31.443	46.824	61.625
AuCu12.5	Area (nm²)	58	99.562	19.783	5774.652	68.885	97.466	137.771
AuCu12.5	Diameter (nm)	58	81.0226	16.42	4699.316	55.214	79.11	112.752
AuCu25	Area (nm²)	97	99.31139	23.8558	9633.2	57.719	99.159	168.718
AuCu25	Diameter (nm)	70	80.484	19.486	7806.942	45.879	80.88	136.87
AuCu40	Area (nm²)	70	88.573	14.615	6200.09	57.069	86.336	130.235
AuCu40	Diameter (nm)	70	72.0188	12.029	5041.319	46.222	70.353	107.049
AuCu50	Area (nm²)	79	58.7533	10.582	4641.514	39.004	57.784	93.899
AuCu50	Diameter (nm)	79	47.705	8.7319	3768.68	31.61	46.585	76.689

3.6 Dynamic Light Scattering (measured ~1 week after synthesis)

DLS measurements (Table 4, Fig. 7a-e) show that the hydrodynamic size and dispersity change depending on the composition. Au NPs had the smallest effective diameter (83.38 nm, PDI 0.305; Fig. 6a). Adding Cu increases the sizes significantly: AuCu25 reaches 635.70 nm (PDI 0.341; Fig. 6c), and AuCu40 has the largest hydrodynamic diameter of 3,535.08 nm (PDI 0.389; Figure 6d), indicating that the particles are highly aggregated in suspension. The average size drops to 580.74 nm at 50% Cu, although the dispersity is at its maximum (PDI 0.719; Fig. 6e), indicating the presence of both aggregates and smaller particles. The sizes obtained from DLS are always bigger than those from FESEM/histogram (Fig. 4, Table 2). The difference is because DLS measures the hydrodynamic diameter, which is the particle core plus any adsorbed surface layers or solvation shells, and is more sensitive to aggregates.

Table 3: Zeta potential and electrophoretic mobility of au and Au-Cu nanoparticles synthesized by PPLAL.

Sample	Zeta Potential (mV)	Mobility (μ/s)/(V/cm)
Au (Pure)	-42.47	-3.32
AuCu12.5	-20.77	-1.62
AuCu25	5.0	0.39
AuCu40	10.13	0.79
AuCu50	-23.85	-1.86

FESEM, on the other hand, solely reveals the physical dimensions of dried particles. Colloids, [32] say that DLS generally overestimates particle size compared to electron microscopy. This is because large particles affect the intensity-weighted average; light scattering depends on particle size; and surface coatings or shape irregularities can also impact the results.

The one-week storage before DLS likely caused some aggregation, which exacerbated the size disparity [33]. Figure 6 shows the Polydispersity Index (PDI) is a dimensionless measure of size distribution in colloids: values < 0.1 indicate a very narrow, monodisperse system; 0.1-0.3 represent a moderate distribution typical for stable nanoparticles; and >0.3 indicate a broad distribution, often linked to aggregation action or multiple particle population.

3.7 UV-Vis Spectroscopy

The UV-Vis spectra of the colloids of Pure Au NPs, and four different compositions ratios of AuCu colloidal nanoparticles are demonstrated in Figure 7. Table 5 are listed the peaks positions and their intensities. The Pure Au colloid shows a strong peak of LSPR band at 521 nm wavelength with maximum intensity at 1.998 abs which establishing the creation of plasmonic characteristic of colloidal Au NPs. While, after adding Cu metal tot eh Pure Au alloy, peak positions of Plasmonic Pure Au Nps moves to extended wavelengths: 568 nm for AuCu12.5 NPs at Abs= 0.186), 579 nm for AuCu25 NPs at Abs = 0.250), 614 nm for AuCu40 NPs at Abs=0.176, and 607 nm for colloidal AuCu50 NPs at Abs= 0.237), as exhibited and listed in Figure 8 and Table 5. The changing in the wavelengths of the peaks with increasing element Cu amounts in Pure Au alloy confirmed that Cu contents changes the light response of the colloidal Au and AuCu particles, supporting the creation of colloidal Au-Cu alloyed nanoparticles [34]-[38].

Due to the UV-Vis resuts provides individual peaks as listed in Table 5, the discussion is focused on wavelength of Surface Plasmon Resonance (λSPR) in the light visible range as the main comparative parameter, while any detailed conclusions about peak width or long-wavelength tailing should be taken from full spectra or supported.

Table 4: DLS results of Au and Au-Cu nanoparticles.

Sample	Effective Diameter (nm)	Polydispersity Index (PDI)	PDI Interpretation
Au (Pure)	83.38	0.305	Moderate distribution, relatively stable
AuCu12.5	1,396.12	0.174	Narrow distribution, uniform aggregates
AuCu25	635.70	0.341	Broad distribution, aggregation present
AuCu40	3,535.08	0.389	Broad distribution, severe aggregation
AuCu50	580.74	0.719	Very broad distribution, mixed populations/instability

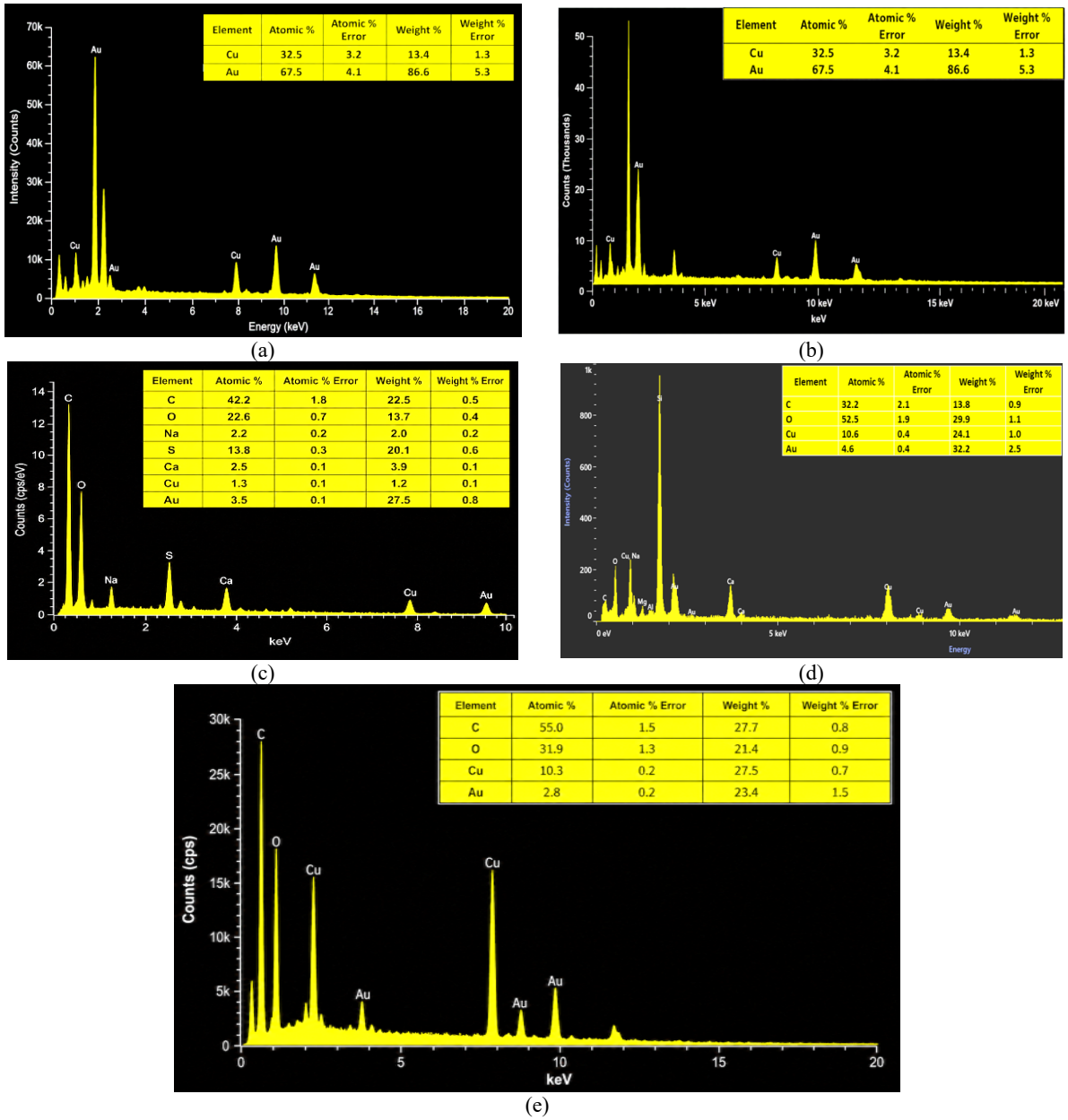

Figure 5: a) EDs plot and mapping images of AuNPs, b) EDs plot and mapping images of AuCu 12.5 wt%, c) EDs plot and mapping images of AuCu 25, d) EDs plot and mapping images of AuCu 40, e) EDs plot and mapping images of AuCu 50.

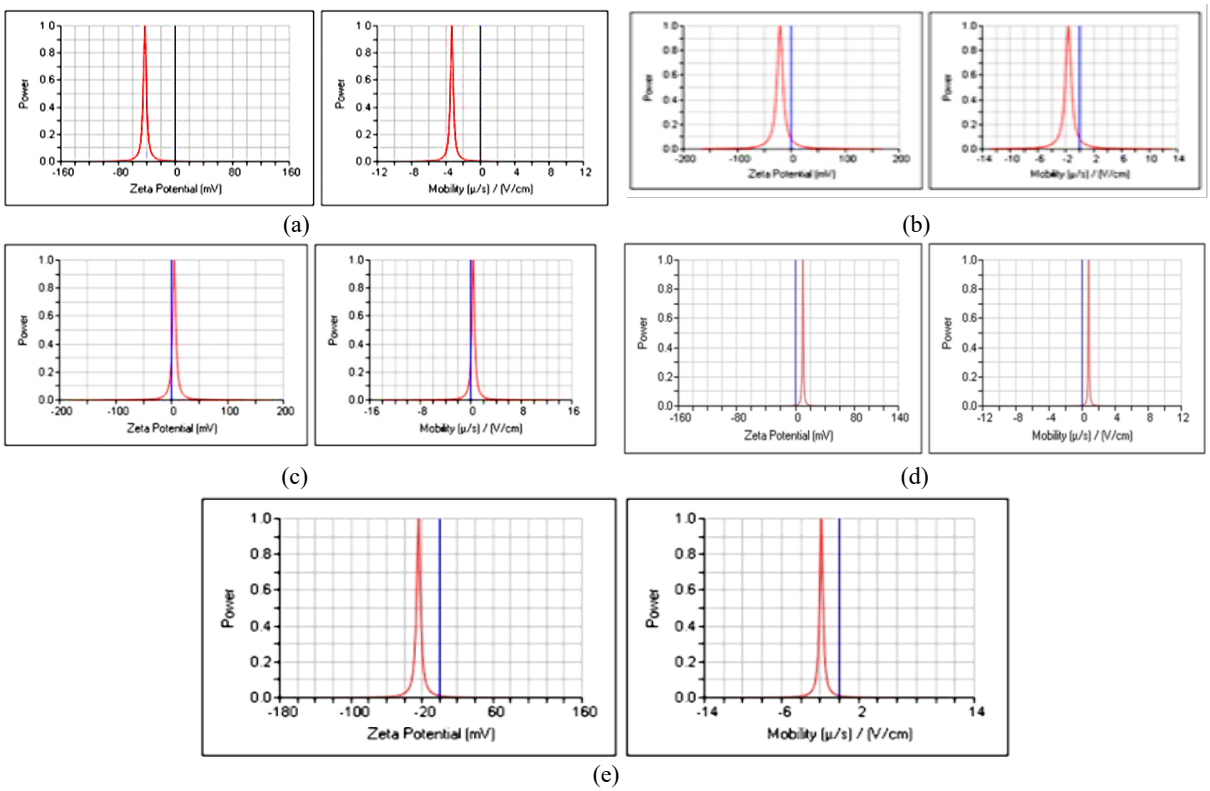

Figure 6: ELS analysis of zeta potential and electrophoretic mobility for Au and Au–Cu nanoparticles synthesized by picosecond pulsed laser ablation in liquid (PPLAL): a) Au, b) AuCu12.5, c) AuCu25, d) AuCu40, and e) AuCu50 nanoparticles.

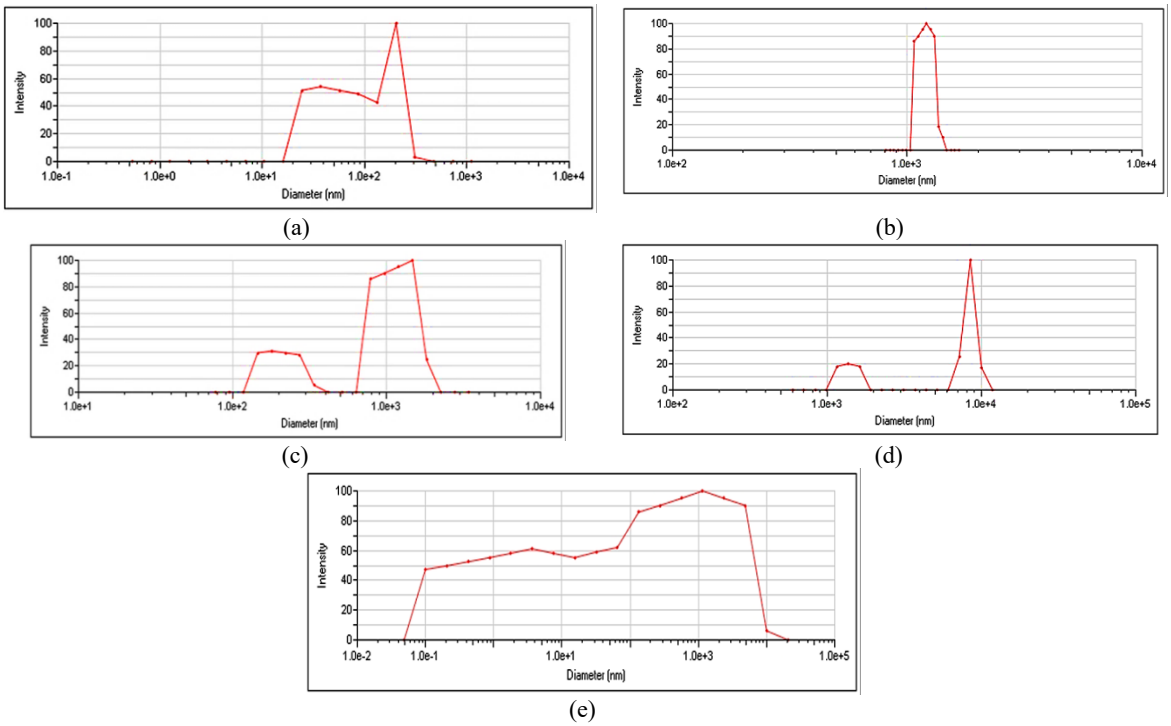

Figure 7: Dynamic light scattering (DLS) intensity size distributions of colloidal Au and Au–Cu nanoparticles synthesized by PPLAL: a) Au, b) AuCu12.5, c) AuCu25, d) AuCu40, and e) AuCu50 nanoparticles.

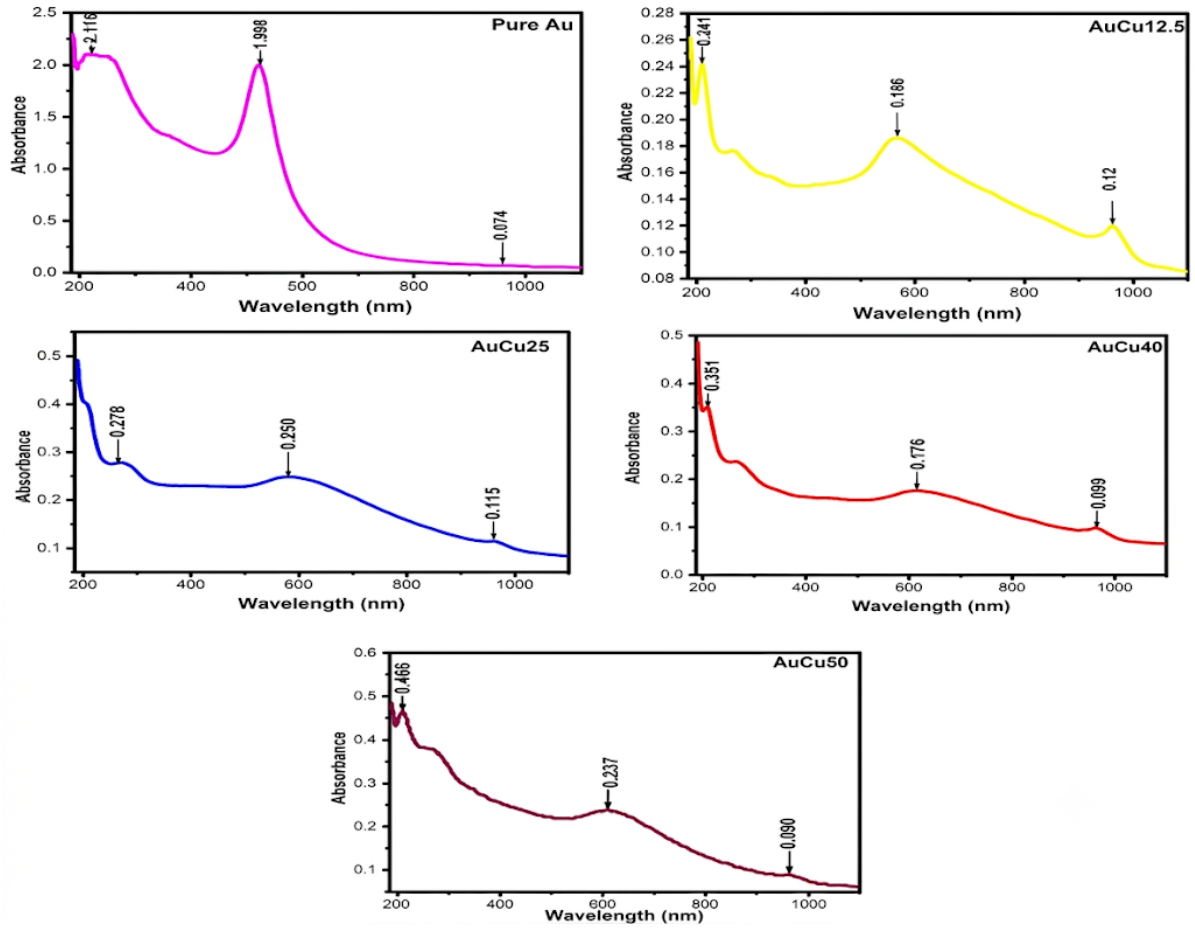

Figure 8: UV-Vis absorption spectra of colloidal nanoparticles prepared by PPLAL in DI water: Au, AuCu12.5, AuCu25, AuCu40, and AuCu50.

Table 5: UV-Vis peak values extracted from instrument reports.

Sample	Major SPR peak λSPR (nm)	Mix Abs at λSPR
Au (Pure)	521.0	1.998
AuCu12.5	568.0	0.186
AuCu25	579.0	0.250
AuCu40	614.0	0.176
AuCu50	607.0	0.237

4 CONCLUSIONS

In this work, we showed how something as simple as changing the gold-copper ratio can reshape the entire story of nanoparticle formation in PPLAL.

As copper entered the lattice, the structure tightened and crystallite sizes shrank, confirming the formation of true Au-Cu solid solutions. On the surface level, this translated into very different particle behaviors: pure gold gave stable, well-dispersed nanoparticles; a small amount of copper encouraged particles to grow larger and stick together; and higher copper contents reversed this, bringing back smaller, more uniform particles. Measurements of surface charge and hydrodynamic size tied these trends directly to colloidal stability, highlighting how mid-range alloys are unstable while Au- and Cu-richer systems regain stability. The LSPR peak movedfrom 521 nm (Au) to 568-614 nm (Au-Cu) depending on composition, demonstrating tunable plasmonic behavior. These results establish Au-Cu NPs alloy composition as a vigorous, surfactant-free parameter for engineering

the structural and colloidal manner of laser-generated bimetallic Au-Cu NPs. These AuCu Alloy NPs have potential applications such as Antibacterial, photo-catalysts, Photo-degradation applications.

ACKNOWLEDGMENT

The authors would like to express their sincere gratitude to the Department of Physics, College of Science, University of Diyala, for their continuous support and provision of the necessary facilities to conduct this research.

REFERENCES

[1] V. D. O. S. Neto, A. J. R. de Castro, G. D. Saraiva, R. F. do Nascimento, et al., "Comprehensive Analytical Chemistry," Comprehensive Analytical Chemistry, vol. 99, pp. 135-162, 2022, [Online]. Available: https://doi.org/10.1016/bs.coac.2021.11.005.

[2] A. Nene, G. Antarnusa, K. Dulta, S. Sadeghzade, L. Wang, C. H. Ravikumar, et al., "ChemPhysMater," ChemPhysMater, vol. 4, pp. 331-343, 2025, [Online]. Available: https://doi.org/10.1016/j.chphma.2025.02.006.

[3] L. Rout, A. Kumar, R. S. Dhaka, G. N. Reddy, S. Giri, and P. Dash, "Appl Catal A: Gen," Applied Catalysis A: General, vol. 538, pp. 107-122, 2017, [Online]. Available: https://doi.org/10.1016/j.apcata.2017.03.017.

[4] R. M. C. R. Ramos and M. D. Regulacio, "ACS Omega," ACS Omega, vol. 6, pp. 7212-7228, 2021, [Online]. Available: https://doi.org/10.1021/acsomega.1c00692.

[5] X. Mi, H. Chen, J. Li, and H. Qiao, "Front Chem," Frontiers in Chemistry, vol. 11, Art. no. 1153936, 2023, [Online]. Available: https://doi.org/10.3389/fchem.2023.1153936.

[6] L.-ur-Rahman, A. Shah, C. Han, and A. K. Jan, "Monitoring of anthracene using nanoscale Au–Cu bimetallic alloy nanoparticles synthesized with various compositions," ACS Omega, vol. 5, pp. 22494-22501, 2020, [Online]. Available: https://doi.org/10.1021/acsomega.0c03104.

[7] Q. Song, Y. Liu, P. Zhang, W. Feng, S. Shi, N. Zhou, et al., "ACS Applied Nano Materials," ACS Applied Nano Materials, vol. 5, pp. 8621-8630, 2022, [Online]. Available: https://doi.org/10.1021/acsanm.2c02152.

[8] M. Sun, A. Wang, M. Zhang, S. Zou, and H. Wang, "ACS Nanoscience Au," ACS Nanoscience Au, vol. 4, pp. 360-373, 2024, [Online]. Available: https://doi.org/10.1021/acsnanoscienceau.4c00035.

[9] D. J. Kim, J. Resasco, Y. Yu, A. M. Asiri, and P. Yang, "Nature Communications," Nature Communications, vol. 5, Art. no. 4948, 2014, [Online]. Available: https://doi.org/10.1038/ncomms5948.

[10] D. S. Idris and A. Roy, "Crystals," Crystals, vol. 13, Art. no. 637, 2023, [Online]. Available: https://doi.org/10.3390/cryst13040637.

[11] A. Nyabadza, E. McCarthy, M. Makhesana, S. Heidarinassab, A. Plouze, M. Vazquez, et al., "Advances in Colloid and Interface Science," Advances in Colloid and Interface Science, vol. 321, Art. no. 103010, 2023, [Online]. Available: https://doi.org/10.1016/j.cis.2023.103010.

[12] V. Kabashin, P. Delaporte, A. Pereira, D. Grojo, R. Torres, T. Sarnet, et al., "Nanoscale Research Letters," Nanoscale Research Letters, vol. 5, Art. no. 454, 2010, [Online]. Available: https://doi.org/10.1007/s11671-010-9543-z.

[13] H. Zeng, X. W. Du, S. C. Singh, S. A. Kulinich, S. Yang, J. He, et al., "Advanced Functional Materials," Advanced Functional Materials, vol. 22, pp. 1333-1353, 2012, [Online]. Available: https://doi.org/10.1002/adfm.201102295.

[14] G. Yang, Laser Ablation in Liquids: Principles and Applications in the Preparation of Nanomaterials. Boca Raton, FL, USA: CRC Press, 2012.

[15] E. Mohebi, S. AdibAmini, A. H. Sari, et al., "Plasmonics," Plasmonics, vol. 19, pp. 75-95, 2024, [Online]. Available: https://doi.org/10.1007/s11468-023-01976-w.

[16] J. Al-Zanganawee, S. Iftimie, T. Mubarak, A. Radu, O. Brincoveanu, S. Antohe, et al., "Journal of Ovonic Research," Journal of Ovonic Research, vol. 12, pp. 95-102, 2016.

[17] A. S. Altowyan, A. M. Mostafa, and H. A. Ahmed, "Optik," Optik, vol. 241, Art. no. 167217, 2021, [Online]. Available: https://doi.org/10.1016/j.ijleo.2021.167217.

[18] D. Sontakke, S. Tiwari, and M. K. Purkait, "FlatChem," FlatChem, vol. 38, Art. no. 100484, 2023, [Online]. Available: https://doi.org/10.1016/j.flatc.2023.100484.

[19] Y. Shih, R. Streubel, J. Heberle, A. Letzel, M. V. Shugaev, C. Wu, et al., "Nanoscale," Nanoscale, vol. 10, pp. 6900-6910, 2018, [Online]. Available: https://doi.org/10.1039/C7NR08614H.

[20] G. Malyavantham, D. T. O'Brien, M. F. Becker, J. W. Keto, and D. Kovar, "Journal of Nanoparticle Research," Journal of Nanoparticle Research, vol. 6, pp. 661-664, 2004, [Online]. Available: https://doi.org/10.1007/s11051-004-3212-z.

[21] X. Mi, R. Wang, Y. Yang, et al., "Plasmonic Au–Cu nanostructures: Synthesis and applications," Frontiers in Chemistry, vol. 11, art. 1153936, 2023, [Online]. Available: https://doi.org/10.3389/fchem.2023.1153936

[22] F. Chang, C. Wang, X. Wu, Y. Liu, J. Wei, Z. Bai, et al., "Materials," Materials, vol. 15, Art. no. 5064, 2022, [Online]. Available: https://doi.org/10.3390/ma15145064.

[23] J. P. Bonasse, M. P. Perich, S. J. Turner, J. E. van der Hoeven, et al., "Nanoscale," Nanoscale, vol. 17, pp. 7100-7113, 2025, [Online]. Available: https://doi.org/10.1039/D5NR00359A.

[24] H. W. Abdullah, T. H. Mubarak, and K. K. Resan, "Science and Technology Indonesia," Science and Technology Indonesia, vol. 9, pp. 806-817, 2024, [Online]. Available: https://doi.org/10.26554/sti.2024.9.4.806-817.

[25] K. S. Mohammed, J. M. Mansoor, J. Alzanganawee, and S. Iftimie, "Journal of Ovonic Research," Journal of Ovonic Research, vol. 17, no. 5, 2021, [Online]. Available: https://doi.org/10.15251/JOR.2021.175.447.

[26] Kittel and P. McEuen, Introduction to Solid State Physics, Hoboken, NJ, USA: John Wiley & Sons, 2018.

[27] G. Pope, "Journal of Chemical Education," Journal of Chemical Education, vol. 74, p. 129, 1997, [Online]. Available: https://doi.org/10.1021/ed074p129.

[28] A. Dahiya, M. Verma, and P. S. Kumar, "Plasmonics," Plasmonics, vol. 17, pp. 2173-2186, 2022, [Online]. Available: https://doi.org/10.1007/s11468-022-01704-w.

[29] K. Choudhury, R. K. Singh, P. Kumar, M. Ranjan, A. Srivastava, and A. Kumar, "Genome-wide identification of the genetic basis of amyotrophic lateral sclerosis," arXiv, Art. no. 1811.01365, 2018.

[30] A. R. West, Solid State Chemistry and Its Applications, Hoboken, NJ, USA: John Wiley & Sons, 2022.

[31] E. Axente, M. Barberoglou, P. G. Kuzmin, E. Magoulakis, P. A. Loukakos, E. Stratakis, et al., "Size distribution of Au NPs generated by laser ablation of a gold target in liquid with time-delayed femtosecond pulses", 2010, [Online]. Available: https://doi.org/10.48550/arXiv.1008.0374.

[32] E. Fazio, B. Gokce, A. De Giacomo, M. Meneghetti, G. Compagnini, M. Tommasini, et al., "Nanomaterials," Nanomaterials, vol. 10, Art. no. 2317, 2020, [Online]. Available: https://doi.org/10.3390/nano10112317.

[33] A. Subhan, A. H. I. Mourad, and Y. Al-Douri, "Nanomaterials," Nanomaterials, vol. 12, Art. no. 2144, 2022, [Online]. Available: https://doi.org/10.3390/nano12132144.

[34] V. Amendola, R. Pilot, M. Frasconi, O. M. Maragò, and M. A. Iatì, "Surface plasmon resonance in gold nanoparticles: A review," Journal of Physics: Condensed Matter, vol. 29, no. 20, Art. no. 203002, 2017, [Online]. Available: https://doi.org/10.1088/1361-648X/aa60f3.

[35] N. E. Motl, A. E. Ewusi-Annan, M. D. Sines, R. E. Schaak, and K. D. Smith, "Au-Cu alloy nanoparticles with tunable compositions and plasmonic properties: Experimental determination of composition and correlation with theory," Journal of Physical Chemistry C, 2010, [Online]. Available: https://doi.org/10.1021/jp107637j.

[36] X. Mi, R. Wang, Y. Yang, et al., "Plasmonic Au-Cu nanostructures: Synthesis and applications," Frontiers in Chemistry, vol. 11, Art. no. 1153936, 2023, [Online]. Available: https://doi.org/10.3389/fchem.2023.1153936.

[37] I. Blakey, Z. Merican, and K. J. Thurecht, "A method for controlling the aggregation of gold nanoparticles," Langmuir, vol. 29, pp. 8266-8274, 2013, [Online]. Available: https://doi.org/10.1021/la401361u.

[38] S. F. Bartolucci, C. M. Gonzalez, et al., "Gold-copper oxide core-shell plasmonic nanoparticles: The effect of pH on shell stability and mechanistic insights into shell formation," Nanoscale Advances, 2024, [Online]. Available: https://doi.org/10.1039/D3NA01000G.